Image Authentication with Tampering Localization Based on Watermark Embedding in Wavelet Domain

Hsuan T. Chang[1], *Chih-Chung Hsu*[2], *Chia-Hung Yeh*[3], *Day-Fann Shen*[1]

[1]Department of Electrical Engineering
National Yunlin University of Science and Technology
Douliu Yunlin, 640 Taiwan ROC

[2] Department of Electrical Engineering
National Tsinhwa University
Hsinchu City, 300 Taiwan ROC

[3]Center for Wireless Multimedia Communications
Department of Electrical Engineering
National Sun Yat-Sen University
Kaoshiung, 804 Taiwan ROC

Abstract

An image authentication and tampering localization technique based on a wavelet-based digital watermarking technique [8] is proposed. To determine whether a given watermarked image has been tampered or not, the similarity between the extracted and embedded watermarks is measured. If the similarity is less than a threshold value, the proposed sequential watermark alignment based on coefficient stamping (SWACS) scheme is used to determine the modified wavelet coefficients corresponding to the tampered region. Then, the morphological region growing and subband duplication (MRGSD) scheme are used to include neighboring wavelet coefficients and then duplicate the wavelet coefficients in other subbands. The experimental results show that the proposed SWACS and MRGSD schemes can efficiently identify different types of image tampering. Moreover, the detection performance of the proposed system on various sizes of the watermark and tampered region is also evaluated.

Keywords: image authentication, tampering localization, digital watermarking, morphology.

February 24, 2009

1 Introduction

Image watermarking techniques recently have received a great deal of attention due to the need of data protection in electronic commerce and surveillance systems [1, 2]. A watermark can be embedded into the image plane directly or in the frequency domain using mathematical transforms such as Fourier transform, discrete cosine transform (DCT), or discrete wavelet transform (DWT) [3]-[7]. Two issues of watermarks, the robustness and fragility, are significant considerations for the use of watermarks in different applications. Among existing techniques, blind watermarking for images [8, 9, 10] is required when the receiver cannot obtain the original images in advance, especially for the image authentication applications. Because images are usually compressed before the transmission or storage, the watermark should be robust to compression. When the extracted watermark is distorted, it is important to distinguish that the distortion is caused from the compression or from illegal tampering. In addition to digital right protection, audio, image, and video authentications are also important applications of watermarking for security or surveillance systems [11, 12, 13]. Fragile watermarks are embedded into video frames or images when they are just generated or during the compression stage. If the image/video content is modified, the fragile watermark is then distorted. Therefore, whether the image has been tampered or not can be identified via the examination of the extracted watermark. Moreover, it is also important to localize the tampered region in images.

Various methods for image authentication with tampering localization have been proposed [14]-[18]. For example, Lin and Chang [14] proposed an effective authentication method based on the invariance of the relationships among DCT coefficients at the same position in separate image blocks. Their method can distinguish JPEG compression from malicious manipulation in images. Hu et. al. [16] proposed a semi-fragile watermarking scheme based on a human-vision-system (HVS) embedding method in the DWT domain to achieve the multi-resolution tamper detection. While tolerating JPEG lossy compression, the proposed method can detect malicious tampers and locate the tampered regions in an image. Celik et al. [18] proposed a lossless authentication framework that can validate the authenticity and integrity of watermarked images without the reconstruction of the original image. In addition to the reduction of computational requirement, this method also enables the public authentication and allows for tamper localization in watermarked images.

Bartollini et al. [11] proposed an image authentication techniques for video surveillance systems. In this method, a pseudo-random number generator with appropriate thresholding is used to yield the watermark sequence. The camera's ID and frame number are used as the watermark key for watermarking a specific frame. Accompanying with the watermark detection, an image denoting the tampered regions of the watermarked image can be obtained. Since the video frames are usually compressed before transmission, the robustness of the watermark to the compression issue is critical. On the other hand, the watermark embedding is performed in the spatial domain rather than in the transform domain. If the pixels in the tampered region do not involve with the watermark information, it will not be detected.

In this paper, an alternative for image authentication based on blind watermarking in the wavelet domain is proposed. When a watermark is embedded in the transform domain, it yields the contribution of the pixel values in the corresponding local positions after the inverse transform. Once the watermarked image is tampered, the pixel values and thus the corresponding wavelet coefficients must be modified such that the extracted watermark will be distorted. When the watermark is embedded in the spatial domain of an image, only the selected pixels contain the watermark information. If the image is tampered only in some small region of the image, the watermark could not be modified and thus the image tampering is not detectable. The proposed method adapts a previous blind watermarking technique [8], which embeds watermarks by the use of the multiple-threshold wavelet coder (MTWC) [21] adopted with successive subband quantization. For the purpose of tampering localization, however, a coefficient stamping scheme which multiplies a random value on each watermark coefficient is proposed. Given the same random seed, an exactly identical stamping sequence can be yielded in the receiver. This combinational method is called the sequential watermark alignment based on coefficient stamping (SWACS) scheme to determine the modified wavelet coefficients. Then, a morphological region growing and subband duplication (MRGSD) method is proposed to include the neighboring wavelet coefficients corresponding to the tampered region and then duplicate to other subbands. By applying the inverse DWT (IDWT) on the determined wavelet coefficients, the tampered region can be determined without using the original image.

The rest of this paper is organized as follows: The blind watermark embedding and extraction technique used in this paper is described in Section 2. Section 3 deals with the proposed SWACS and MRGSD methods for watermark alignment and tampering detection. The experimental results for different types of image tampering and the precision analysis of the proposed method are given Section 4. Finally, Section 5 concludes this paper.

2 Blind Watermarking based on Multiple-Threshold Wavelet Coder

Figure 1 shows the block diagram of the blind watermark embedding and extraction processes. Suppose that the image $f(x, y)$ is of size $h \times w$. To embed a watermark $w(x, y)$ in the image, the image is first transformed into the frequency domain by the use of DWT [24]. The significant subbands are first selected according to the largest coefficient values in the subbands. Next the watermark message are embedded into the significant coefficients that are selected according to the rule shown in Ref. [8]. Then the watermark is embedded into the selected coefficients in some significant subbands of DWT. After the watermark is embedded, the watermarked image can be obtained by the use of the IDWT. As shown in Fig. 1(b), the watermark extraction process basically is similar to that of the watermark embedding process. The extraction of the watermark is blind, i.e., the original image is not referred while retrieving the watermark.

2.1 Watermark Embedding

This watermark embedding comprises of two stages [8]: the significant coefficient search and the adaptive watermark casting and retrieval. At the first stage, an image is wavelet transformed with the 7/9 filter [23] into 4-level subbands. Suppose that the wavelet coefficients in each subband are Gaussian distributed with zero mean and variance σ^2 [8]. The significant subbands are selected as they contain more energy, i.e., the variance σ^2 is greater than the threshold value T_s. The procedures are summarized as follows:

1. For each subband s, the initial threshold T_s is set as one half of its maximum absolute value of all coefficients $C_s(u,v)$. That is, $T_s = |C_{\max,s}|/2$. Let all coefficients be un-selected.

2. Excluding the DC term, the subband with the maximum value of $\beta_s T_s$ is selected, where β_s is the weighting factor of subband s and $|\beta_s| \leq 1$.

3. By examining all the un-selected coefficients $C_s(u,v)$ in the selected subbands, the coefficients greater than the current threshold T_s are selected as the significant coefficients. The watermark is then casted in these selected coefficients.

4. If all the watermark symbols are yet casted, the threshold in the subband s is updated as $T_s^{\text{new}} = T_s/2$.

5. Repeat Steps 2–4 until the condition shown in Step 4 is satisfied.

In the MTWC, each coefficient $C_s(u,v)$ in the subband s can be expressed as

$$C_s(u,v) = sgn \times (a_0 \frac{T_s}{2^0} + a_1 \frac{T_s}{2^1} + \ldots + a_b \frac{T_s}{2^b} + \ldots), \tag{1}$$

where the symbol "sgn" represents the sign value of the coefficient $C_s(u,v)$, i.e.,

$$sgn = \begin{cases} 1, & \text{if } C_s(u,v) \geq 0 \\ -1, & \text{if } C_s(u,v) < 0 \end{cases} \tag{2}$$

and a_b is the binary bit at the bth bit plane. Note that $b = 0$ denotes the most significant bit plane layer. For the binary watermark $w(x, y)$ whose size is $n \times m = N$ and pixel values are either 255 or 0, let

$$W(k) = \begin{cases} 1, & \text{if } w(x, y) = 255 \\ -1, & \text{if } w(x, y) = 0 \end{cases} \quad (3)$$

where $k = nx + y$. The watermark casting on the selected coefficient is performed by the following equation:

$$C'_{s,b,k}(u, v) = sgn \times \Delta_p(C_{s,b}(u, v)) + \alpha_s \beta_s T_{s,b} W(k), \quad (4)$$

where $T_{s,b}$ and $C_{s,b}$ denote the threshold value and the wavelet coefficient on the subband s in the bth bit plane, respectively, and α_s $(0 < \alpha_s \leq 1)$ is the scaling factor in the subband s for adjusting the robustness of the watermark. The operation $\Delta_p(\cdot)$ is defined as

$$\Delta_p(C_{s,b}(u, v)) = (1 + 2p\alpha_s)T_{s,b}, \quad (5)$$

and the parameter p is determined as

$$p = \arg\min_{p'} \text{DIS}_{s,b,p'}(u, v), \quad (6)$$

where p' is an integer between one and $(2\alpha_s)^{-1}$ and the distance $\text{DIS}_{s,b,p}(u, v)$ between $C_{s,b}(u, v)$ and $\Delta_p(C_{s,b}(u, v))$ is defined as

$$\text{DIS}_{s,b,p}(u, v) = |\Delta_p(C_{s,b}(u, v)) - |C_{s,b}(u, v)||. \quad (7)$$

Note that the modified coefficient $C'_{s,b,k}(u, v)$ should be smaller than $C_{s,b,\max}$ such that the later one will not be changed. Thus the correct extraction of the watermark can be guaranteed. With this restriction, the criteria on the parameters α_s and β_s can be expressed as

$$\begin{cases} \text{True}, & \text{for } (sgn + sgn \times 2p\alpha_s + \alpha_s \beta_s W(k)) < 2, \\ \text{False}, & \text{Otherwise.} \end{cases} \quad (8)$$

Here the "True" denotes that the watermark $W(k)$ can be embedded by using the parameters α_s and β_s. On the other hand, the "False" denotes the case in which both the parameters cannot be used for watermark embedding.

2.2 Watermark Extraction

To extract the embedded watermark from the received image $f_w^*(x, y)$, similar procedures shown in Eqs. (2)–(4) are performed. Let $C^*_{s,b,\max}(u, v)$ denote the selected maximum significant coefficient in the subband s and bth bit plane of the DWT of the received image. We also define that $T^*_{s,b} = |C^*_{s,b,\max}(u, v)|/2$. Suppose that the selected coefficients $C^*_{s,b,\max}(u, v)$ and $C_{s,b,\max}(u, v)$ in the original and received images are about the same. That is, $C^*_{s,b,\max}(u, v) \approx C_{s,b,\max}(u, v)$ and thus $T^*_{s,b} \approx T_{s,b}$. Referring to Eq. (4) for the watermark embedding, the watermark extraction can be performed by

$$\begin{aligned} \alpha_s \beta_s T^*_{s,b} W^*(k) &= C^*_{s,b}(u, v) - sgn \times \Delta_{p^*}(C_{s,b}(u, v)) \\ &= C^*_{s,b}(u, v) - sgn \times (1 + 2p^* \alpha_s) T^*_{s,b} \end{aligned} \tag{9}$$

and

$$W^*(k) = \frac{C^*_{s,b}(u, v) - sgn \times (1 + 2p^* \alpha_s) T^*_{s,b}}{\alpha_s \beta_s T^*_{s,b}}. \tag{10}$$

Obviously, the extracted watermark coefficient $W^*(k)$ is a real number within the range $[1, -1]$. The coefficient can be transformed to the value between zero and 255 by

$$w^*(x, y) = \text{round}(\frac{W^*(k) + 1}{2} \times 255), \tag{11}$$

where $x = k$ mode m, $y = k - mx$ and the "round(z)" denotes the operation of taking the integer closest to the value z. Thus the extracted watermark is the union of all transformed coefficients. The original watermark is a binary image. However, the extracted watermark from the wavelet domain is grayscale. Therefore, a binarization process with an adequate threshold value is required.

To verify the extracted watermark, the cross-correlation of the extracted and the original watermarks is used to represent their similarity SIM$[w(x, y), w^*(x, y)]$, which is defined as

$$\text{SIM}[w, w^*] = \frac{< w, w^* >}{< w, w >} = \frac{\sum_{x=0}^{n-1} \sum_{y=0}^{m-1} w(x, y) w^*(x, y)}{\sum_{x=0}^{N-1} \sum_{y=0}^{M-1} w^2(x, y)} \leq 1. \tag{12}$$

Here SIM$[w, w^*] = 1$ denotes that both watermarks are exactly identical. As shown in Eq. (11), the coefficients in the extracted watermark are graylevels between 0 and 255, while the original coefficients are binary. If the watermarked image is not attacked, the coefficients $C^*_{s,b}$ should be very close to the original ones $C_{s,b}$. That is, the similarity SIM$[w(x, y), w^*(x, y)]$ should be as close as unity.

An image is usually compressed before the transmission or storage. The watermark extracted from the decoded image will be distorted due to the lossy compression. Let the watermarked image quality be represented by the peak signal-to-noise ratio (PSNR). Figures 2(a) and 2(b) show the original image and the watermark, respectively. The JPEG-compressed watermarked image (PSNR=39.45 dB) and the extracted watermark are shown in Figs. 2(c) and 2(d), respectively. As shown in Fig. 2(d), the extracted watermark is obviously distorted. High similarity is a necessary condition for further tampering detection and localization.

In general, important images are usually stored with a uncompressed form. Therefore, lossy compression schemes such as JPEG are seldom applied on the images. (Even used, the high-quality mode is preferred.) If the compression is used to save storage space or to reduce the transmission bandwidth, lossless schemes are recommended. As for the application of image authentication, the capability of the robustness to lossy compression is no longer required because there will be an original watermark in the receiver for comparison purpose. In order to detect image tampering from the extracted watermark, the previous blind watermarking scheme is adapted and will be shown in next section.

3 Tampering Detection and Localization

With the blind watermarking scheme shown above, whether or not the received image has been tampered can be determined by measuring the similarity between the original and extracted watermarks. If the similarity is less than a threshold value (set to be 0.8 in this paper), the received image is considered as being tampered by illegal users. To perform the tampering detection and localization for the malignant modification in images, the SWACS and MRGSD methods are proposed. Figure 3 shows the block diagram of the proposed image authentication and tampering localization method. Given a tampered watermarked image $f_w^*(x, y)$, the watermark is extracted and converted into 1-D binary sequence $W^*(k)$. By comparing with the original watermark sequence $W(k)$ based on the proposed SWACS method, the wavelet coefficients $C_T(u, v)$ corresponding to the tampered region are determined. By applying the proposed MRGSD method on the selected coefficients and then performing the IDWT on the whole coefficients, a reference image $f_w^R(x, y)$ is obtained. Finally, the difference image $f_{\text{error}}(x, y)$ between the tampered image $f_w^*(x, y)$ and the reference image $f_w^R(x, y)$ is then used to estimate the tampered region in the image. The detailed operation in each block will be described as follows.

The extracted watermark will be distorted when the watermarked image has been tampered. Since the maximal coefficient $C_{s,b,\max}(u, v)$ in each subband might be modified during the tampering, thus we adapt the original scheme shown in Section 2.2 to solve this problem. There are three possible cases in extracting the watermark coefficients: (1) an extra coefficient, (2) a lost coefficient, (3) extra and lost coefficients happen together. However, if there are multiple and adjacent "-1" and/or "1" in any case above, it is hard to determine the exact locations which correspond to the image tampering. Figures 4(a) and 4(b) show the examples of the first two cases. As shown in Fig. 4(a) , $W(k)$ and $W^*(k)$ denote the kth original and extracted watermark coefficients, respectively. And $W^{**}(k)$ denotes the possible modifications to recover the original watermark coefficients. Although it is easy to find that there is an extra "1" coefficient in $W^*(k)$, the exact position of the extra coefficient cannot be exactly located. For the case of a lost coefficient due to the tampering in the image, a similar situation can be observed in Fig. 4(b). Therefore, one cannot correctly determine the tampering positions just by comparing the original and the extracted watermarks. To overcome this problem, here a coefficient stamping scheme which can successfully determine the coefficients corresponding to the image tampering is proposed.

3.1 Sequential Watermark Alignment based on Coefficient Stamping Scheme

To correctly extract every watermark coefficient and detect the position of tampering, the embedded coefficients are no longer -1 or 1. Instead, each coefficient is modified by the use of a random number V to become the value within the range [-1, 1] during the embedding processing. Equation (4) now is rewritten as

$$C'_{s,k}(u,v) = sgn \times \Delta_p(C_s(u,v)) + \alpha_s \beta_s T_s W(k) V(k), \tag{13}$$

where $V(k)$ is a random sequence of the same length with the watermark sequence $W(k)$. In addition to that each number is unique, the values of the coefficients are normalized to be within a small range $0.7 \sim 1$. Similarly, the condition $C'_{s,b,k}(u,v) < C_{s,b,\max}$ should also be hold in Eq. (13). Now the new equation for watermark extraction becomes

$$\hat{W}^*(k) = \frac{C'_{s,k}(u,v) - sgn \times (1 + 2p^* \alpha_s) T^*_s}{\alpha_s \beta_s T^*_s V(k)}. \tag{14}$$

The difference value ΔV of two consecutive random values, $V(k)$ and $V(k+1)$, significantly affects the coefficient extraction process. For example, two consecutive values $V(k) = 0.7$ and $V(k+1) = 0.85$ lead to that the difference between two consecutively extracted coefficients $\hat{W}^*(k)$ and $\hat{W}^*(k+1)$ is proportional to $1/0.7 - 1/0.85 = 0.25$. That is, $\hat{W}^*(k) = \hat{W}^*(k+1) \times 1.25$ and thus the correct sequential relationship of the watermark coefficient can be correctly identify by introducing the random number $V(k)$. However, the extracted watermark coefficients will be difficult to be identified if the difference value ΔV is small. To solve this problem, we can set a criterion to ensure that the difference value ΔV is larger than a threshold value 0.2, so that the missed $W(k)$ can be easily found in the next stage. For a random value $V(k)$, if the value $V(k+1)$ cannot satisfy the criterion, the value $V(k+1)$ is discarded and the following values $V(k+2), V(k+3), \ldots$ are tested until the criterion is satisfied. When the watermarked image has been tampered, the values of extracted watermark coefficients $\hat{W}^*(k)$ will be quite different from the original coefficients $W(k)$. To determine that whether the coefficient is abnormal, the criterion

$$\begin{cases} 1, \text{ if } \mid W(k) - \hat{W}^*(k)\mid > D_{\text{th}} \\ 0, \text{ Otherwise} \end{cases} \tag{15}$$

is employed, where D_{th} denotes a threshold value. Basically the threshold value D_{th} should be greater than one and is set to be 1.5 in our experiments.

For an abnormal coefficient $\hat{W}^*(k)$, the average error values $E(k)$ of consecutive L decoded coefficients are determined as follows:

$$E(k) = \frac{1}{L}\sum_{i=k}^{k+L} |W(i) - \hat{W}^*(i)|. \tag{16}$$

A large average value $E(k)$ represents that the decoded coefficient $\hat{W}^*(k)$ is a truly abnormal coefficient and then a seeking process is applied to determine the position of insertion or deletion. Suppose that there is an insertion or deletion inside the position range $[k, k+L]$; total $2L$ values of $E(k)$ for an insertion or deletion case happened at each position in this range are determined. The position i^* can be determined by seeking the minimum value of all $E(k)$ values. That is,

$$i^* = \arg\min_i \left(\frac{1}{L}\sum_{i=k}^{k+L} |W(i) - \hat{W}^*(i)| \right), \tag{17}$$

where i represents the position where the insertion or deletion happened. The case of insertion or deletion on the wavelet coefficient $\hat{W}^*(k)$ and the corresponding position i^* can be determined. In our experiment, the L value is set to be 10, which is large enough to identify the insertion or deletion position. When the criterion cannot be reached, the watermark extraction will be terminated. This situation could happen at when the tampered region is quite large such that the embedded watermark has been seriously destroyed. Therefore, the tampered region cannot be identified accordingly.

After performing the SWACS scheme on the extracted and original watermarks, most of the wavelet coefficients that have been altered in the tampered image are detected. By the use of the inverse DWT, these coefficients will be transformed to further determine the tampered region in the image. However, as mentioned in the case (2), there are some corresponding wavelet coefficients which may not be detected. In order to significantly emphasize the tampered region, the proposed MRGSD scheme is then employed.

3.2 Wavelet Coefficient Duplication based on Morphological Region Growing Scheme

To signalize the tampered region with the detected wavelet coefficients, their positions in a specific lower subband are duplicated to the corresponding positions in the same and higher subbands. For a detected coefficient appearing at the sth HL subband, the other coefficients located at the same position in the LL, HH, and LH subbands are selected. Next, for the higher or lower levels of subbands, the coefficients corresponding to the same position will also be selected. The positions of the selected wavelet coefficients could be very sparse, which lead to the detected tampered region shown in a broken structure. Mathematical morphology has been successfully employed to localize the tampered region in images [11]. Therefore, morphological close operations are then applied to all the selected coefficients to include the neighboring coefficients such that a complete region of the image tampering can be expected. Note that the structure elements for dilation and erosion operations are 7×7 and 5×5, respectively. All the wavelet coefficients located at the selected positions at all subbands will then be employed to the tampered region determination instead of only using the originally detected coefficients.

For each coefficient $C_T(u,v)$ located in the identified position, some modification is required to obtain a reference image $f_w^R(x,y)$ such that the tampered region can be determined by the use of the difference image between the reference and tampered images, $f_w^*(x,y)$ and $f_w^R(x,y)$, respectively. According to our empirical test results, the modified coefficient $C_R^*(u,v)$ can be determined as

$$C_R^*(u,v) = \begin{cases} C_T(u,v) \times 0.5, & \text{if } C_T(u,v) \text{ is selected;} \\ C_T(u,v), & \text{if } C_T(u,v) \text{ is not selected.} \end{cases} \tag{18}$$

With the modified coefficients, the reference image $f_w^R(x,y)$ can be constructed by applying the

IDWT on $C_R^*(u,v)$. That is,

$$f_w^R(x,y) = \text{IDWT}\{C_R^*(u,v)\}. \tag{19}$$

Obviously, the difference image corresponding to the modified wavelet coefficients will predict the tampered region in the image. Therefore, the error image $f_{\text{error}}(x,y)$ between the tampered image $f_w^*(x,y)$ and the constructed reference image $f_w^R(x,y)$ can be calculated by

$$f_{\text{error}}(x,y) = 255 - |f_w^*(x,y) - f_w^R(x,y)|, \tag{20}$$

which is then binarized by a given threshold value for easily displaying the differences between two images. Finally, an estimated tampered region in the tampered image can be obtained. Compared with the tampered image, we can localize and identify the tampered region and content, respectively.

3.3 Precision and Security Analysis

To evaluate the precision of the proposed method, the detected tampered region is compared with the actually tampered region. Let the pixel numbers in the covered tampered region, in the actually tampered region, and in all the detected region be denoted as N_c, N_t, and N_a, respectively. Two factors are used to evaluate the detection accuracy of the proposed method on image tampering:

(1) The coverage ratio (C_r) is defined as

$$C_r = \frac{N_c}{N_t}; \tag{21}$$

(2) The redundancy ratio (R_r) is defined as

$$R_r = \frac{N_a}{N_c}. \tag{22}$$

Both factors are desired as close as unity.

It is very important that the watermark cannot be extracted by an intruder before he wants to tamper the watermarked image. Therefore, the watermark embedding and extraction processes should not be open to the public. In addition, the parameters (α_s, β_s, T_s, the watermark $W(k)$, and the random sequence $V(k)$) used in the proposed system are sensitive to the accuracy of the watermark extraction. (Actually the security is mainly guaranteed by the use of a long watermark and a long random sequence.) As shown in Eq. (14), some small modification on these parameters can lead to very large difference on the determined result of the watermark coefficient. Moreover, consider the random sequence which is of the same length ($l = m \times n$) with the watermark sequence. Even though that the watermark size is known, the possible combinations of the random sequence will be $(n \times m)^r$, where r denotes the number of the bits required to represent the real number in the random sequence. For example, if the watermark size is 44×44 and the number $r = 5$, then there are total $2^{20} \times 11^{10}$ possible combinations. Considering the further combinations with other parameters, the security level is high enough to prevent the brute force attacking.

4 Experimental Results and Discussion

In computer experiments, a watermarked image of size 512×512 shown in Fig. 7(a) and the watermark of size 44×44 shown in Fig. 2(b) are used to test the proposed methods. The parameters used in the experimental are given as $\alpha_s = 0.25,\ \beta_s = 1$, and $V(k)$ is within the range [0.7, 1]. Figure 5 shows the PSNR values of the watermarked images which embed the different sizes of the watermark. When the size of watermark is only 22×22, the PSNR values is close to 39 dB. As the size increases to 33×33, the PSNR values decrease rapidly. For a large size 88×88 of watermark, the PSNR value is still higher than 33 dB, which is still acceptable quality.

Figure 6 shows the detection result of abnormal wavelet coefficients when the watermarked image has been tampered. The differences between the extracted and the original watermark coefficients for two cases are illustrated. If the watermarked image is not tampered, all the difference values between two watermark coefficients, $|W(k) - W^*(k)|$, are small (< 0.5). After the image has been tampered, some of the difference values $|W(k) - \hat{W}^*(k)|$ are greater than one. Thus the abnormal coefficients can be detected using the SWACS scheme. The undetected coefficient, of course, will affect the synchronization with the sequence $V(k)$. Some wavelet coefficients are missed and several false coefficients are detected. The impact of this effect appears as imperfect detection on the tampered region. That's why the tampered region cannot be perfectly detected in the proposed method.

Figure 7(b) shows the tampered image $f_w^*(x, y)$, in which an extra mark is inserted comparing with the watermarked image shown in Fig. 7(a). By using the proposed SWACS scheme, the wavelet coefficients corresponding to the tampered region can be detected through the comparison between the original and extracted watermarks. Figure 7(c) shows the extracted positions of the originally detected and copied wavelet coefficients in different subbands. These wavelet coefficients are modified based on Eq. (1) and then are joined with other coefficients to be inverse wavelet transformed to obtain a revised image $f_w^R(x, y)$. Figure 7(d) shows the binarized error image between the tampered and the revised images. Figure 7(e) shows the binarized error image between the revised and the embedded images. By using the proposed MRGSD scheme, the determined tamper region can be obtained. Figure 7(f) shows that the determined region can cover the actual region. The coverage and the redundancy ratios are $C_r = 1.0$ and $R_r = 3.16$, respectively.

Two different types of tampering in the F-16 images are also considered in our simulation. Figure 8(a) shows that part of the text "US AIR" printed on the jet plane has been artificially removed from the image. By using the proposed SWACS and MRGSD methods on the tampered image, the detected tampered region can be obtained and is shown in Figure 8(b), in which the original tampered region is also shown for comparison. Figure 8(c) shows that a rectangular region in the plane has been blurred. As shown in Fig. 8 (d), the proposed method can successfully detect the tampered region as well. The corresponding coverage and redundancy ratios for Figs. 8(b) and 8(d) are $\{C_r = 1.0, R_r = 4.6\}$ and $\{C_r = 0.9, R_r = 5.2\}$, respectively. From the results shown in Figs. 7 and 8, different types of tampering or modifications can be correctly detected and localized in the corresponding regions. Therefore, the tampered part in the image can be easily identified by the use of the proposed SWACS and MRGSD methods.

Consider the types of image tampering shown in Figs. 7(b), 8(a), and 8(c), in which the sizes of tampered region are 34×26, 44×44, and 40×40, respectively. Table 1 shows the effects on the C_r and R_r precisions under different types of image tampering and different scales of the tampered region. For the type of image tampering shown in Fig. 7(b), almost all of the entire tampered region can be identified (i.e., $C_r \approx 1$) even when the scale of tampered region is 350%. On the other hand, the redundancy ratio R_r increases a lot when the scale is only 10%. The tampered region can be correctly identified but the size of detected region is much larger than the real one. A similar trend happens for the type of image tampering shown in Fig. 8(c). The only difference is that the coverage ratio C_r decreases a lot when the scales are 250% and 350%. For the type of image tampering shown in Fig. 8(a), the coverage ratio C_r is less than 0.5 as the scales are not less than 150%, which means that the detection performance is not good enough when the tampered region increases. Table 2 shows the effects on the C_r and R_r precisions under different types of image tampering and different sizes of the watermark. For the two types of image tampering shown in Figs. 7(b) and 8(c), coverage ratios R_r can be greater than 10 only when the size of watermark is 88×88. When the size of the watermark is less than 44×44, the detection of text remove in Fig. 8(a) is inefficient because the coverage ratios are small. There is no regularity on the redundancy ratio R_r in this type of image tampering.

To investigate the sensitivity of α_s or β_s on the detected tampered region, the following experiments are performed. Let $\alpha_s = 0.1$ and $\beta_s = 1$ and the watermarked image be not tampered. No tampered region should be detected if all the parameters are correct. If an incorrect α_s value is used, then the extracted watermark will be incorrect and thus some false tampered region will be detected. Table 3 shows the ratios of the area of false tampered region to the original image size under different α_s values. When the α_s value is 0.105, the 0.9% region size of the image is falsely detected as the tampered region. Therefore, some minor deviation on α_s could lead to different authentication results.

Finally, a special case of attack on the smooth region in the watermarked F-16 image is used to test the proposed schemes. As can be seen in Fig. 9(a), a smaller aircraft is inserted into the uniform cloudy region in the F-16 image with a smoothing process on the aircraft boundary. Figure 9(b) shows the ground truth of the tampered region in the image. With the same parameters in the watermark embedding/extraction process, only the tail of the inserted smaller aircraft can be detected. Figs. 9(c) and 9(d) show the detected tampered region and its corresponding position in the tampered image, respectively. Note that the grayscale values of the pixels in the fuselage are similar to that of its neighboring cloud. The fuselage cannot be detected because the corresponding wavelet coefficients are smaller than the Nth wavelet coefficient. However, this attack only works in the smooth region in the watermarked image because very few wavelet coefficients can be selected to embed the watermark bits. Therefore, the tampering region will be undetectable because the value of the maximum wavelet coefficient of the inserted object is less than that of the Nth significant wavelet coefficient in this region. To prevent this problem, a large N value is required in the proposed method. Under this condition, the tampering effect will be negligible. That is, the inserted object could be almost invisible if the value N is large enough and the attacker's purpose may not be achieved.

5 Conclusion

In this paper, a blind watermarking scheme is adopted to perform the image authentication and tampering localization in the receiver. According to the similarity of the extracted watermark, whether or not the received image is tampered can be determined. To detect the tampering and localize the tampered region in the image, the SWACS and MRGSD methods are proposed to efficiently determine the positions of the modified pixels in the distorted watermark and to estimate the possible tampered region, respectively. The experimental results verify that the proposed system can successfully perform the image authentication and tampering localization for different types and various sizes of image tampering. To further improve the precision performance of the detected results, adequately selecting the watermark size N and determining the system parameters in the proposed methods would be helpful.

6 Acknowledgment

This work is partly supported by the National Science Council, Taiwan R.O.C. under contract NSC 97-2221-E-224-057. The authors appreciate the valuable comments from anonymous reviewers.

References

[1] C.-T. Hsu and J.-L. Wu, "Hidden digital watermarks in images," *IEEE Transactions on Image Processing*, vol. 8, no. 1, pp. 58–68, Jan. 1999.

[2] C.I. Podilchuk and E.J. Delp, "Digital watermarking: algorithms and application," *Signal Processing Magazine, IEEE,* vol. 18, no. 4, pp. 33–46, July 2001.

[3] S.D. Lin and C.-F. Chen, "A robust DCT-based watermarking for copyright protection," *IEEE Transactions on Consumer Electronics,* vol. 46, no. 3, pp. 415–421, Aug. 2000.

[4] X. Kang, J. Huang, Y.Q. Shi, and Y. Lin, "A DWT-DFT composite watermarking scheme robust to both affine transform and JPEG compression," *IEEE Transactions on Circuits and Systems for Video Technology*, vol. 13, no. 8, pp. 776–786, Aug. 2003

[5] H. Yuan and X.-P. Zhand, "A multiscale fragile watermark based on the Gaussian mixture model in the wavelet domain," *2004 IEEE International Conference on Acoustics, Speech, and Signal Processing (ICASSP)*, vol. 3, pp. 413–416, Montreal, Canada, May 2004

[6] A. Briassouli, P. Tsakalides, and A. Stouraities, "Hidden messages in heavy-tails: DCT domain watermark detection using alpha-stable model," *IEEE Transactions on Image Processing*, vol. 7, no. 4, pp. 700–715, Aug. 2005

[7] S.-H. Wang and Y.-P. Lin, "Wavelet tree quantization for copyright protection watermarking," *IEEE Transactions on Image Processing*, vol. 13, no. 2, pp. 154–165, Feb. 2004

[8] H.-J. Mike Wang, P.-C. Su, and C. -C. Jay Kuo, "Wavelet-based digital image watermarking," *Optics Express*, vol. 3, no. 12. pp. 491–496, Dec. 1998

[9] P.-C. Su and C. -C. Jay Kuo, "Blind digital watermark for cartoon and map images," *Proceedings of SPIE*, vol. 3657, pp. 296–306, April 1999

[10] P.H.W. Wong, O.C. Au, and Y.M. Yeung, "Novel blind multiple watermarking technique for images," *IEEE Transactions on Circuits and Systems for Video Technology*, vol. 13, no. 8, pp. 813–830, Aug. 2003

[11] F. Bartollini, A. Tefas, M. Barni and I. Pitas, "Image authentication techniques for surveillance applications", *Proceedings of the IEEE*, vol. 89, no. 10, pp. 1403–1418, Sept. 2001

[12] M.D. Swanson, Bin Zhu, and A.H. Tewfik, "Multiresolution scene-based video watermarking using perceptual models," *IEEE Journal on Selected Areas in Communications,* vol. 16, no. 4, pp. 540–550, May 1998.

[13] D. Kirovski and H.S. Malvar, "Spread-spectrum watermarking of audio signals," *IEEE Trans. on Signal Processing,* vol. 51, no. 4, pp. 1020–1033, Apr. 2003.

[14] C.-Y. Lin and S.-F. Chang, "A Robust Image Authentication Method Distinguishing JPEG Compression from Malicious Manipulation," *IEEE Trans. on Circuits and Systems for Video Technology*, vol. 11, no. 2, pp. 153–168, Feb. 2001.

[15] M.U. Celik, G. Sharma, E. Saber, and A.M. Tekalp, "Hierarchical watermarking for secure image authentication with localization," *IEEE Transactions on Image Processing*, vol. 11, no. 6, pp. 585–595, Jun. 2002

[16] J. Hu, J. Huang, D. Huang, and Y.Q. Shi, "Image fragile watermarking based on fusion of multi-resolution tamper detection," *Electronics Letters*, vol. 38, no. 24, pp.1512–1513, Nov. 2002

[17] H.D. Knowles, D.A. Winne, C.N. Canagarajah, and D.R. Bull, "Image tamper detection and classification using support vector machines," *IEE Proceedings on Vision, Image and Signal Processing*, vol. 151, no. 4, pp. 322–328, 30 Aug. 2004

[18] M.U. Celik, G. Sharma, E. Saber, and A.M. Tekalp, "Lossless watermarking for image authentication: a new framework and an implementation," *IEEE Transactions on Image Processing*, vol. 15, no. 4, pp. 1042–1049, Apr. 2006

[19] C. Rey ahd J.L. Dugelay, "A Survey of Watermarking Algorithms for Image Authentication," *EURASIP Journal on Applied Signal Processing*, vol. 2002, no. 6, pp. 613–621, 2002

[20] W. Zhu, Z. Xiong, and Ya-Qin Zhang, "Multiresolution watermarking for images and video," *IEEE Transactions on Circuits and Systems for Video Technology,* vol. 9, no. 4, pp. 545–550, June 1999.

[21] H.-J. Wang and C. -C. Jay Kuo, "A multi-threshold wavelet coder (MTWC) for high fidelity image compression," *Proceedings of IEEE 1997 International Conference on Image Processing,* vol. 1, pp. 652–655, Oct. 1997

[22] A.Tefas and I. Pitas, "Image authentication and tamper proofing using mathematical morphology," *European Signal Processing Conference* (EUSIPCO'2000), Tampere, Finland, vol.3, pp. 1681–1684, 5-8 Sept. 2000

[23] M. Rabbani and R. Joshi, "An overview of the JPEG2000 still image compression standard," *Signal Processing: Image Communication*, vol. 17, no. 1, pp. 3–48, January 2002

[24] M. Antonini, M. Barlaud, P. Mathieu, and I. Daubechies, "Image coding using wavelet transform," *IEEE Transactions on Image Processing*, vol. 1, no. 2, pp. 205–220, Apr. 1992.

Table 1: The effects on the two precisions C_r and R_r under different types of image tampering and different scales of the tampered region.

	Fig. 7(b)		Fig. 8(a)		Fig. 8(c)	
Scale	C_r	R_r	C_r	R_r	C_r	R_r
10%	1.0	25.6	1.0	13.4	1.0	58.4
25%	1.0	6.9	0.84	10.6	1.0	23.1
50%	1.0	3.5	0.90	5.0	1.0	8.8
100%	1.0	3.2	1.0	4.6	0.90	5.2
125%	1.0	5.4	0.99	4.4	1.0	4.7
150%	1.0	3.4	0.44	2.1	0.94	3.7
250%	0.98	2.4	0.47	3.1	0.58	3.2
350%	0.95	2.2	0.38	2.8	0.68	3.3

Table 2: The effects on the two precisions C_r and R_r under different types of image tampering and different sizes of the embedded watermark.

	Fig. 7(b)		Fig. 8(a)		Fig. 8(c)	
Size	C_r	R_r	C_r	R_r	C_r	R_r
22×22	1.0	2.6	0.46	2.7	0.99	3.5
33×33	1.0	3.0	0.57	8.2	0.93	3.9
44×44	1.0	3.2	1.0	4.6	0.90	5.2
55×55	1.0	3.2	0.84	5.1	0.91	5.2
66×66	1.0	2.7	0.75	8.5	1.0	6.0
77×77	1.0	3.4	0.86	4.7	1.0	7.7
88×88	1.0	12.5	0.74	7.5	1.0	11.5

Table 3: The sensitivity of α_s on the detection results of the tampered region.

α	0.2	0.1	0.11	0.105	0.101
Ratio	23.3%	0	15.4%	1.9%	0.9 %

Figure Captions:

Figure 1: The block diagrams for watermark (a) embedding and (b) extraction in the wavelet domain.

Figure 2: (a) The original image and (b) the embedded watermark. (c) The watermarked image (PSNR = 39.45 dB) and (d) the extracted watermark.

Figure 3: The block diagrams of the proposed image authentication and tampering localization method.

Figure 4: Two possible alignment results between the original and the extracted watermarks: (a) An extra coefficient is found and discarded; (b) A coefficient is lost and should be inserted.

Figure 5: The PSNR values of the watermarked images with different watermark sizes.

Figure 6: The difference values between the original watermark coefficients and the extracted coefficient before and after image tampering.

Figure 7: (a) The watermarked image; (b) The tampered watermarked image in which a logo covers the tail; (c) The extracted watermark which is seriously distorted; (d) The detected coefficients in the wavelet domain; (e) The wavelet coefficient at the same and lower subbands are predicted from the original coefficients; (f) The comparison between the determined region and actually tampered regions.

Figure 8: Two other examples for tampering detection and localization: (a) The F-16 image is tampered by erasing part of the text; (b) The comparison between the detected and actual tampered regions; (c) The F-16 image is tampered by blurring part the texture; (d) The comparison between the detected and actual tampered regions.

Figure 9: (a) An example of inserting an small aircraft in the uniform cloudy region in the F-16 image. (b) The ground truth of the tampered region in the image; (c) The tampered region detected from the proposed method. (d) The corresponding position of the detected region in the tampered image.

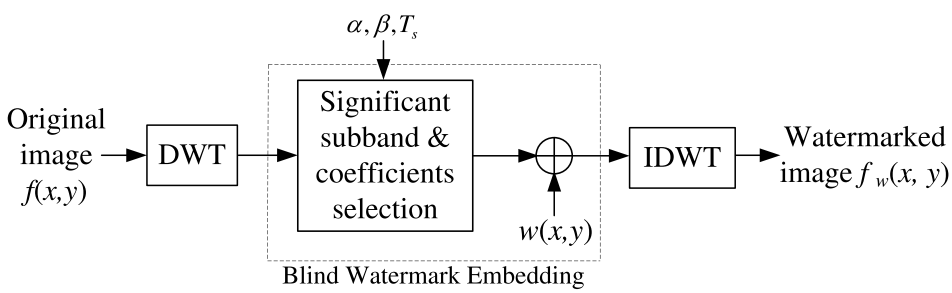

(a)

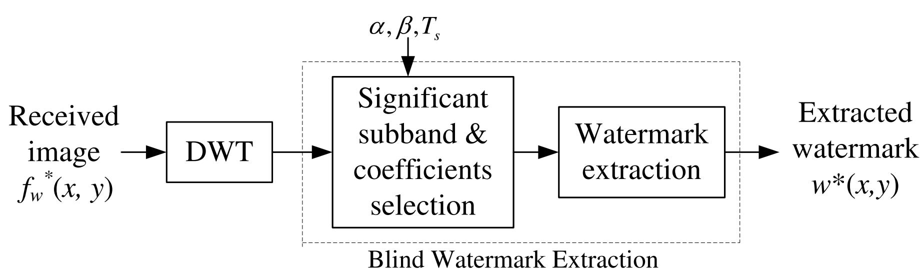

(b)

Figure 1: The block diagrams for watermark (a) embedding and (b) extraction in the wavelet domain.

Figure 2: (a) The original image and (b) the embedded watermark. (c) The watermarked image (PSNR = 39.45 dB) and (d) the extracted watermark.

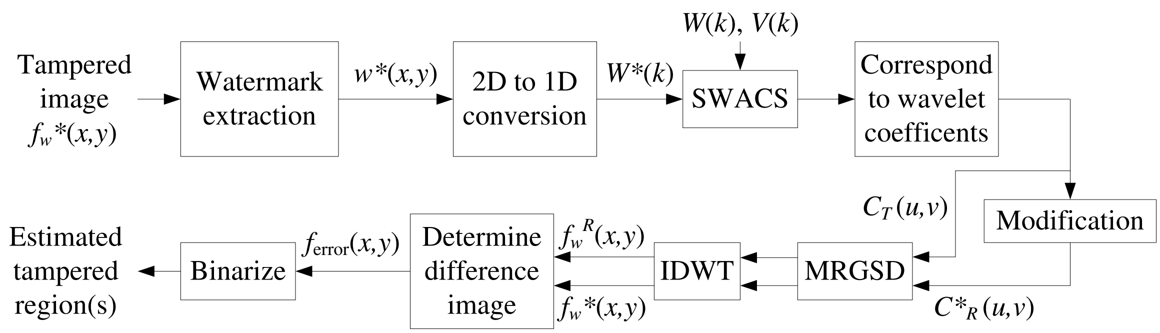

Figure 3: The block diagrams of the proposed image authentication and tampering localization method.

 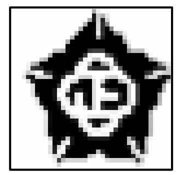

(a) (b)

 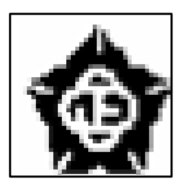

(c) (d)

Figure 4: Two possible alignment results between the original and the extracted watermarks: (a) An extra coefficient is found and discarded; (b) A coefficient is lost and should be inserted.

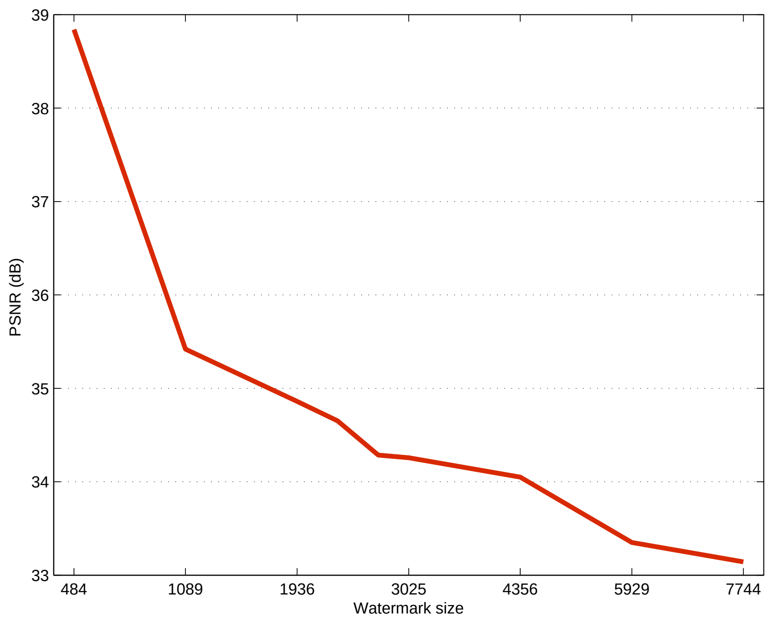

Figure 5: The PSNR values of the watermarked images with different watermark sizes.

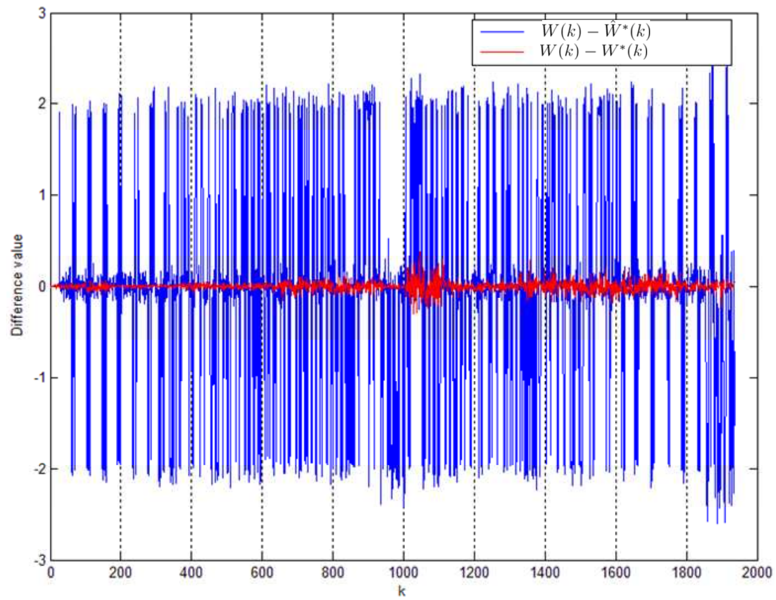

Figure 6: The difference values between the original watermark coefficients and the extracted coefficient before and after image tampering.

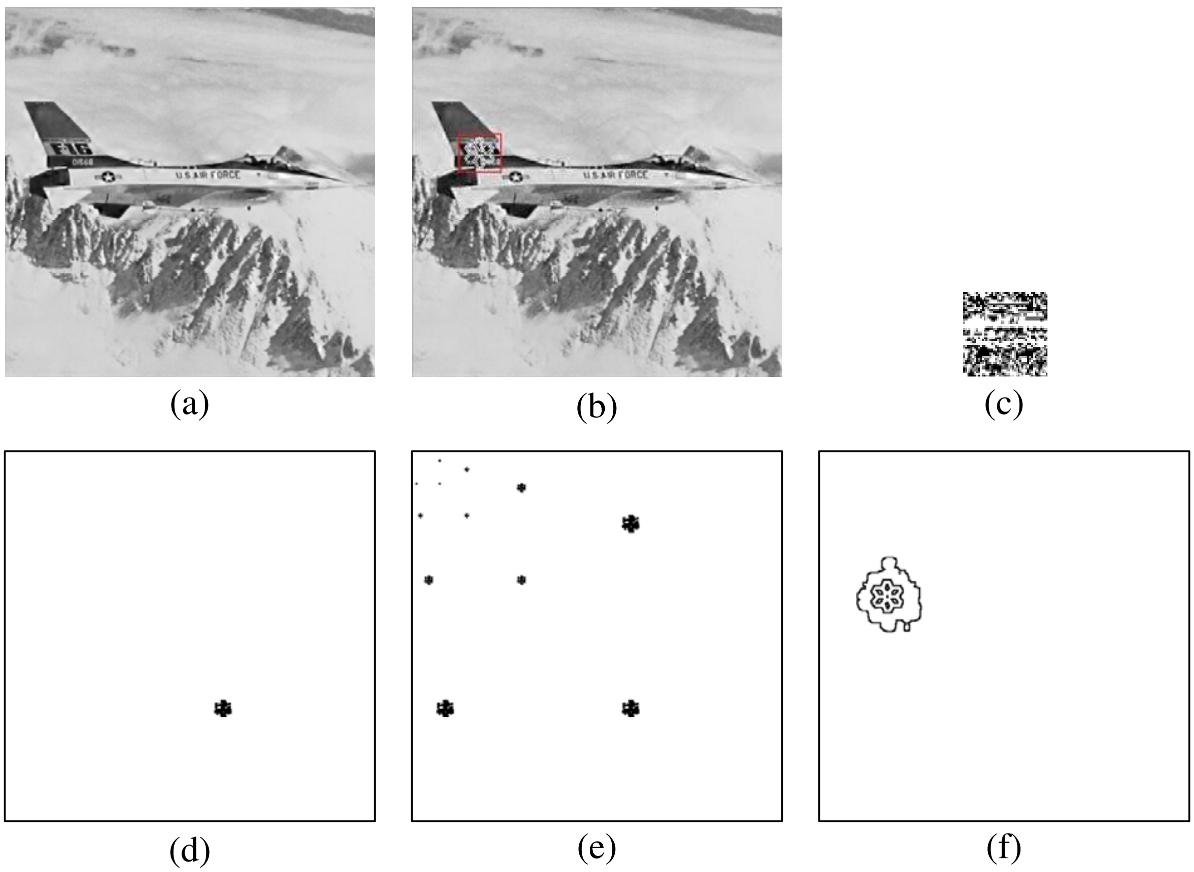

Figure 7: (a) The watermarked image; (b) The tampered watermarked image in which a logo covers the tail; (c) The extracted watermark which is seriously distorted; (d) The detected coefficients in the wavelet domain; (e) The wavelet coefficient at the same and lower subbands are predicted from the original coefficients; (f) The comparison between the determined region and actually tampered regions.

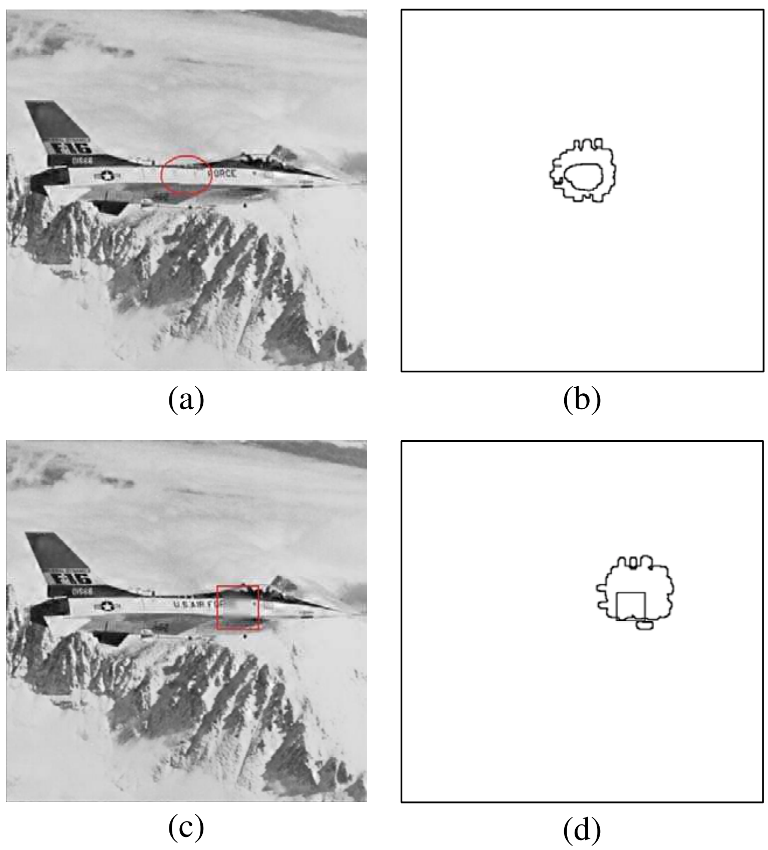

Figure 8: Two other examples for tampering detection and localization: (a) The F-16 image is tampered by erasing part of the text; (b) The comparison between the detected and actual tampered regions; (c) The F-16 image is tampered by blurring part the texture; (d) The comparison between the detected and actual tampered regions.

(a) (b) (c) (d)

Figure 9: (a) An example of inserting an small aircraft in the uniform cloudy region in the F-16 image. (b) The ground truth of the tampered region in the image; (c) The tampered region detected from the proposed method. (d) The corresponding position of the detected region in the tampered image.